Korean J. Chem. Eng., 32(5), 837-844 (2015)
DOI: 10.1007/s11814-014-0277-y

pISSN: 0256-1115
eISSN: 1975-7220

Agro-industrial waste-mediated synthesis and characterization of gold and silver nanoparticles and their catalytic activity for 4-nitroaniline hydrogenation

Preeti Dauthal and Mausumi Mukhopadhyay†

Department of Chemical Engineering, S.V. National Institute of Technology, Surat-395007, Gujarat, India
(*Received 10 March 2014 • accepted 15 September 2014*)

Abstract–The biosynthesis of gold (Au-NPs) and silver nanoparticles (Ag-NPs) using agro-industrial waste *Citrus aurantifolia* peel extract as a bio-reducing agent is reported. Catalytic activity of nanoparticles (NPs) was evaluated for hydrogenation of anthropogenic pollutant 4-nitroaniline (4-NA). Both synthesized NPs were nearly spherical and distributed in size range of 6-46 and 10-32 nm for Au-NPs and Ag-NPs, respectively. XRD analysis revealed face centered cubic (fcc) structure of both NPs. ζ potential value obtained from colloidal solution of Au-NPs and Ag-NPs was −28.0 and −26.1 mV, respectively, indicating the stability of the NPs in colloidal solution. FTIR spectra supported the role of citric and ascorbic acids of peel extract for biosynthesis and stabilization of NPs. The biosynthesized NPs exhibited excellent catalytic activity for hydrogenation of 4-NA in the presence of $NaBH_4$.

Keywords: *Citrus aurantifolia*, Nanoparticles, Biosynthesis, Hydrogenation, Nitroaniline

INTRODUCTION

The synthesis and application of noble metal nanoparticles (NPs) is the subject of enormous interest due to its large surface area-to-volume ratio and modified structure [1,2]. This is particularly significant for gold (Au-NPs) and silver nanoparticles (Ag-NPs), which have strong surface plasmon resonance (SPR) oscillations [3,4]. Due to the interface-dominated properties, these metals NPs hold considerable promise for different catalytic applications such as hydrogenation of aromatic nitro compounds [5] and oxidation of benzyl alcohol [6].

Unique optical, electrical and excellent catalytic properties of these noble metal NPs have spurred interest in developing different methodologies for the synthesis. The chemical reduction method is a feasible approach. Elevated temperature, high pressure, cost, environmental toxicity, biological hazards and utilization of toxic chemicals are the main disadvantages. With the growing interest in minimization of waste, a requirement of an energy efficient, eco-friendly, biocompatible and sustainable process through the implementation of the fundamental green chemistry principles is desirable nowadays.

The bio-inspired synthesis of metal NPs using different plant parts such as leaf [7], bark [8], root [9], flower [10], seed [11] and fruit [12] has been reported so far. The naturally available agricultural waste fruit peels have not been investigated much for the synthesis of metal NPs. Fewer works are reported for metal NPs synthesis using peel extract [13,14]. Motivated by the potential catalytic application of noble NPs and the state-of-art of the biosynthesis, *Citrus aurantifolia* peel extract is initially screened for reduction of number of metal ions like copper, iron, selenium, nickel, ruthenium, palladium, platinum, gold and silver metal ions at room temperature. However, only Au-NPs and Ag-NPs are biosynthesized by *C. aurantifolia* peel extract. This is because biosynthesis usually works well for metal ions with large positive electrochemical potential such as Au and Ag ions [15,16]. In addition, silver or gold particles are relatively inert and stable, and thus easily synthesized through biological route [17]. However, rapid oxidation of cheaper iron and copper particles in aquatic environment of biological extract complicates their synthesis through biological route [17-19].

Au-NPs and Ag-NPs were reported earlier as catalyst for various nitroaromatic compounds hydrogenation [12,20,21] due to their active surface atoms and high surface energy properties [22]. Use of biomass-supported nanocatalyst in this direction eliminates the need of additional catalyst matrix, as the process of nano-colloids incorporation on external polymeric support significantly attenuates the catalytic activity of NPs [23,24]. Furthermore, the inert behavior of biomass in the absence of NPs provides additional benefits. Thus biomass-supported nanocatalysts, despite using costly metals like Au and Ag, greatly reduce the overall cost incurred in bioremediation with an added advantage of eco-friendliness. Therefore, biosynthesis of Au-NPs and Ag-NPs is presented using agro-industrial waste *C. aurantifolia* peel extract as reducing agent and their catalytic activity is also evaluated for 4-nitroaniline (4-NA) hydrogenation to 4-phenylenediamine (4-PDA). This is mainly used as ingredients in industrial dyes [25] and as rubber antioxidants [26].

The biosynthesis and catalytic activity of biosynthesized Au-NPs and Ag-NPs is instantly traced by UV-visible spectroscopic methods. The as-synthesized NPs are characterized by transmission electron microscopy (TEM), X-ray diffraction (XRD), dynamic light scattering (DLS), energy-dispersive X-ray spectroscopy (EDX) and Fourier transform infrared spectroscopy (FTIR).

EXPERIMENTAL

1. Materials

All reagents of analytical grade were used as received without

†To whom correspondence should be addressed.
E-mail: mmu@ched.svnit.ac.in, mausumi_mukhopadhyay@yahoo.com

any further purification. Tetrachloroauric (III) acid ($HAuCl_4 \cdot 3H_2O$), silver nitrate ($AgNO_3$), 4-nitroaniline ($C_6H_6N_2O_2$) and sodium borohydride ($NaBH_4$) was procured from HiMedia Pvt. Ltd, Mumbai, India. Fresh peels of *C. aurantifolia* were collected from the local market of Surat.

2. Synthesis of Au-NPs and Ag-NPs

The peel extract of *C. aurantifolia* used in the biosynthesis of NPs was prepared from 50 g thoroughly washed *C. aurantifolia* peel in a 500 mL Erlenmeyer flask and boiled with 250 mL double distilled deionized water at 60 °C for 10 min. The resultant crude extract was filtered with Whatman filter paper no. 40. The filtered extract was stored at 4 °C for further study. Then 900 mL of 1×10^{-3} M aqueous solution of $HAuCl_4 \cdot 3H_2O$ (pH 2.9) and $AgNO_3$ (pH 4.8) were reduced using 100 mL of peel extract at room temperature (28±2 °C) in two different reactions. Both reaction mixtures were kept at 500 rpm for 2 min. The effect of interaction time in the SPR of colloidal Au-NPs and Ag-NPs was evaluated up to 24 h. These NPs were separated from reaction mixture by centrifugation at 10,000 rpm for 10 min and washed several times with distilled water and acetone and dried in an oven at 60 °C.

3. Catalytic Hydrogenation of 4-NA using NPs

In the typical experiment, 4 mL of 12×10^{-3} M 4-NA solution was added to the 0.8 mL aqueous $NaBH_4$ (1×10^{-1} M) solution. The reaction mixture was partitioned into two parts (each part about 2.4 mL aliquots). Finally, 100 µL of ultrasonically dispersed Au-NPs and Ag-NPs (0.1 mg/mL) suspension in double distilled water was introduced (resulting in a constant metal loading of 10.0 µg) in the above two reaction mixtures separately at 28±2 °C. Time-dependent absorption spectrum was recorded at every 2 min interval. The effect of concentration of NPs on the catalytic hydrogenation of 4-NA was also evaluated with 5, 10, 15, 20 and 25 µg of both NPs at room temperature.

4. Characterization of the Au-NPs and Ag-NPs

The time-dependent analysis of Au-NPs and Ag-NPs biosynthesis along with its catalytic activity for 4-NA hydrogenation was kinetically monitored by periodic sampling of the 2 mL aliquots, and optical absorbance was recorded on a UV-visible spectrophotometer (DR 5000, HACH, USA) at different time intervals. Deionized water was used as a blank. Hydrodynamic size distribution and zeta (ζ) potential measurements of colloidal NPs were carried out using DLS (Zetasizer Nano ZS90, Malvern, UK). The size and morphology of the synthesized NPs were determined by TEM (CM200, Philips, UK) operated at an accelerating voltage of 100 kV with resolution 2.4 Å. Crystalline structure, composition as well as particle sizes of the synthesized NPs were analyzed by X-ray diffractometer (X'pert pro, PANalytical, Holland) operated with a voltage of 45 kV and current of 35 mA with Cu-K_α radiation (K=1.5406 Å). The scanning range (2θ) was selected from 30° to 80° at 0.045°/min continuous speed. Elemental analysis of NPs was performed using energy dispersive spectroscopy (EDS) (X-Max 80 mm^2, Oxford Instrument) coupled with scanning electron microscopy (SEM) (JSM-7600F, JEOL, Japan) operated at an accelerated voltage of 20 kV. FTIR spectral measurements of both NPs and *C. aurantifolia* extract were in the range of 600 and 3,600 cm^{-1}, by using FTIR (MAGNA 550, Nicolet, USA) in the diffuse reflectance mode at a resolution of 2 cm^{-1} in KBR pellets.

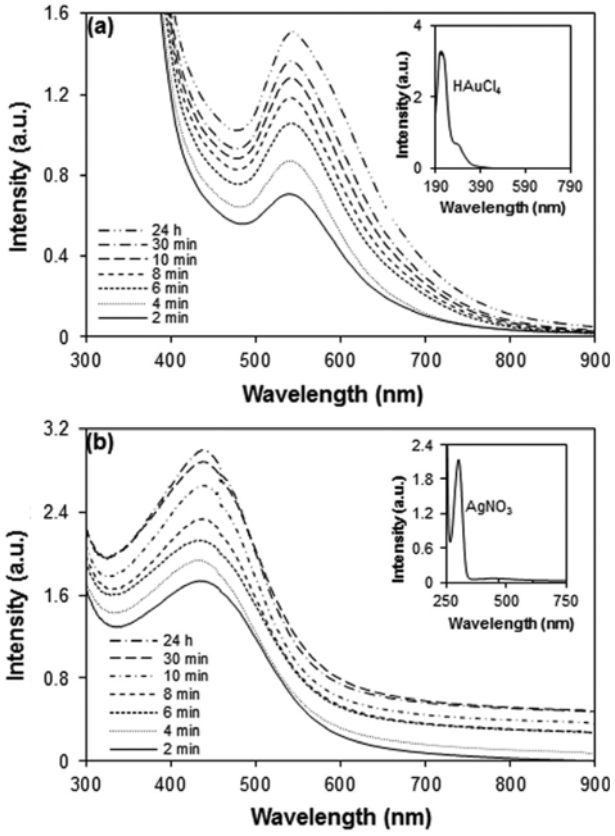

Fig. 1. Time-dependent UV-visible spectra of (a) Au-NPs (b) Ag-NPs using *C. aurantifolia* peel extract at room temperature. Inset in (a) represents the absorption spectra of $HAuCl_4 \cdot 3H_2O$ and in (b) $AgNO_3$.

RESULTS AND DISCUSSION

1. UV-visible Spectra Analysis

In the present study, aqueous $HAuCl_4 \cdot 3H_2O$ solution initially showed a strong absorption peak at 217 nm and a shoulder at 287 nm (inset picture in Fig. 1(a)). Similarly, $AgNO_3$ salt solution showed a strong absorption band at around 290 nm (inset picture in Fig. 1(b)). These peaks were due to charge transfer between the metal ions and corresponding ligands in aqueous solutions. After mixing 1×10^{-3} M $HAuCl_4 \cdot 3H_2O$ and $AgNO_3$ solution with *C. aurantifolia* peel extract, these peaks completely vanished within 2 min. This indicated the reduction of Au^{3+} and Ag^+ starting within 2 min. The UV-visible spectra recorded for Au-NPs and Ag-NPs synthesis with aqueous extract of *C. aurantifolia* as a function of reaction time are represented in Fig. 1(a) and 1(b), respectively.

Ruby red and orange color were observed in colloidal Au-NPs and Ag-NPs, respectively. This color change was due to the surface plasmon resonance (SPR) vibration of metal NPs, arising from collective oscillation of free conduction electrons induced by an interacting electromagnetic field [27]. The appearance of single symmetric SPR bands at 540 and 437 nm indicated the formation of uniformly dispersed spherical Au-NPs and Ag-NPs, respectively. As Mie's theory suggests, the single SPR peak was expected in the absorption spectra of spherical NPs while, higher number of SPR peaks indi-

cated the lower symmetry of the NPs [28].

The SPR bands in the colloidal solution of Au-NPs and Ag-NPs remained at about 540 and 437 nm, respectively, throughout the reaction period of 24 h. However, the band intensity increased steadily. This indicated the stability and uniformity in particles size distribution throughout the reaction periods as the position of SPR band influenced by the particle size, shape, local refractive index and its interaction with medium. Therefore, stability of the Au-NPs and Ag-NPs was also due to the capping of NPs with phytoconstituents, released by the peel extract to the reaction medium. Stability

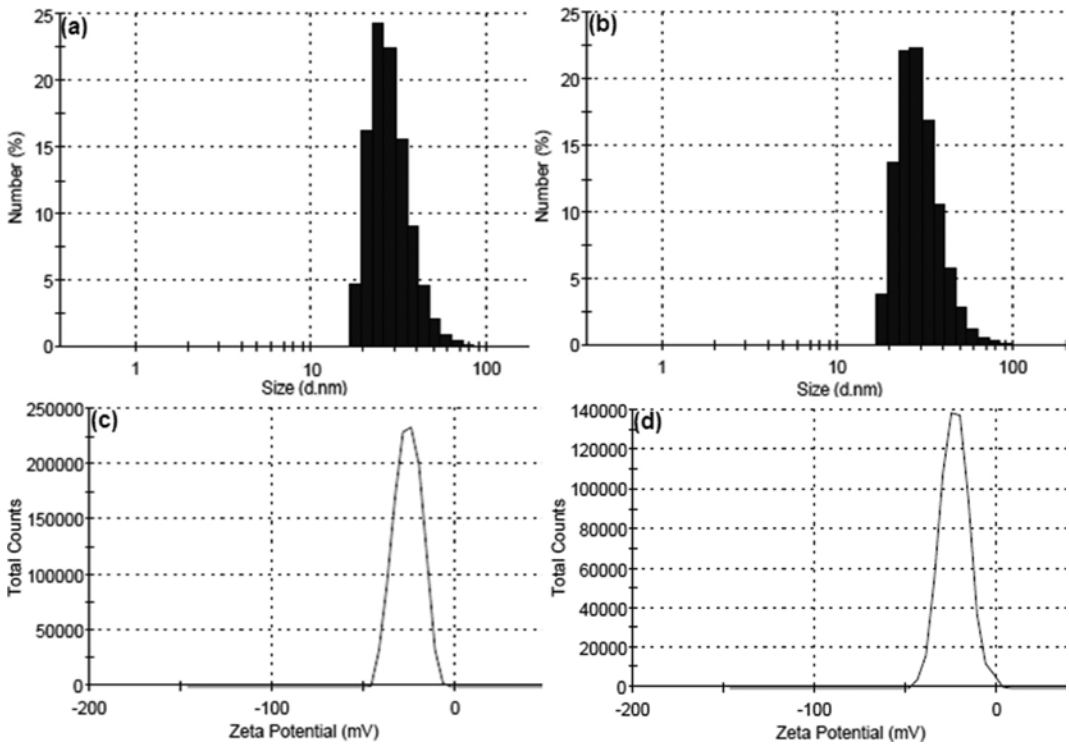

Fig. 2. DLS spectra of (a) Au-NPs (b) Ag-NPs, corresponding ζ potential distribution of (c) Au-NPs (d) Ag-NPs.

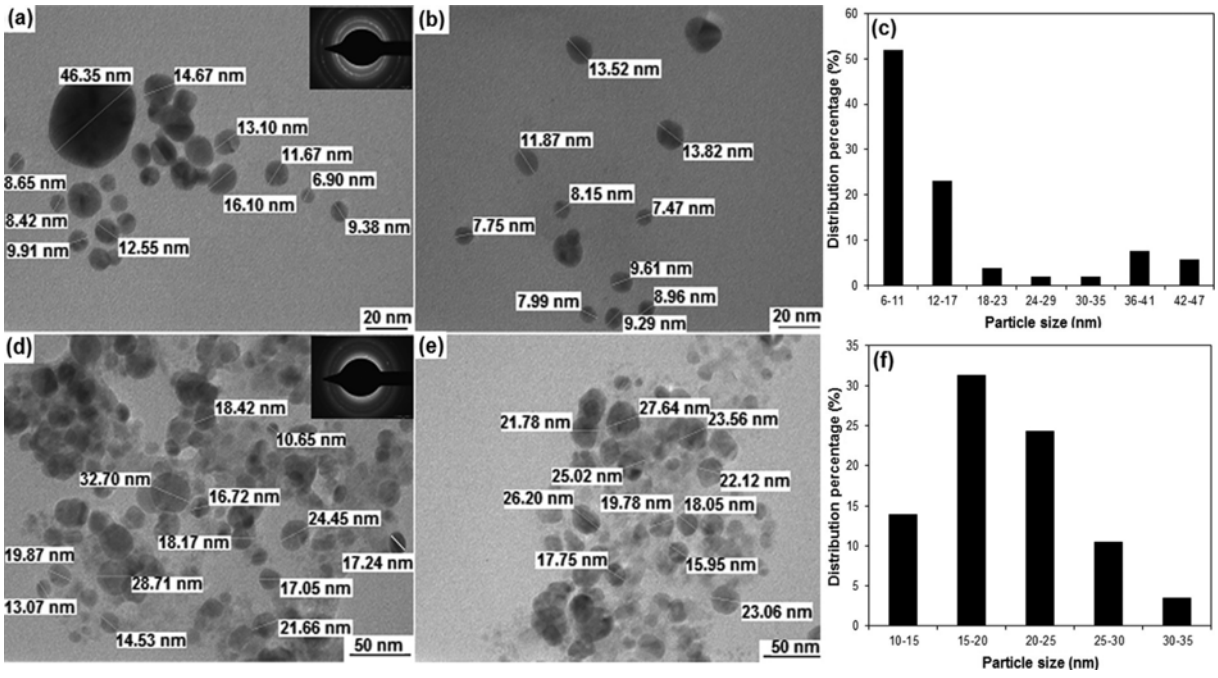

Fig. 3. TEM image of (a)-(b) Au-NPs (c) size distribution histogram of Au-NPs (d)-(e) Ag-NPs (f) size distribution histogram of Ag-NPs (inset shows corresponding SAED pattern).

of NPs was also confirmed by measured negative ζ potential value of NPs in colloidal solution.

The sharp drop in reaction time from several hours to few minutes indicated the commercial viability of this bio-fabrication process. This was the fastest method of biosynthesis in comparison to the conventional studies with other plants and microbial cultures. The time required for the conventional synthesis of NPs from other plants varied from 2 to 4 h.

2. Particle Size and ζ Potential Analysis

The DLS spectra represented Z-average diameter 69.69 nm for Au-NPs with polydispersity index (PdI) 0.249 (Fig. 2(a)). However, 48.03 nm Z-average diameter was observed for Ag-NPs with PdI 0.176 (Fig. 2(b)). The ζ potential value for Au-NPs and Ag-NPs was −28.0 and −26.1 mV, respectively. This high-negative ζ potential value provided the necessary repulsive force and ensured a high energy barrier between the NPs to withhold agglomeration, thereby improving the stability of NPs in colloidal solution.

3. Transmission Electron Microscopy Analysis

TEM was also used to determine the size and morphology of NPs. TEM images of Au-NPs (Fig. 3(a), (b)) indicated particles were relatively uniform in size with spherical shape. Au-NPs were distributed in the size range of 6-46 nm with an average particle size of 16 nm. The average size and size distribution of NPs were calculated using ImageJ software. Histogram obtained from TEM image of Au-NPs suggested that, majority of the particles (>74%) resided in size range of 6-17 nm and few large sizes anisotropic Au-NPs were also observed (Fig. 3(c)). However, spherical shapes Ag-NPs were obtained in the range of 10-32 nm with average particle size of 20 nm and majority of particles (>55%) fall in size range of 15-25 nm (Fig. 3(d), (e), (f)). These NPs were also analyzed by electron diffraction directly on the microscope. The electron diffraction patterns (inset picture in Fig. 3(a) and (d)) showed bright circular concentric rings, resulting from the random orientation of crystal planes, suggested crystalline nature of synthesized NPs.

The fabrication of large size anisotropic Au-NPs were formed at later stage, lack the protective biomolecules and, hence, thermodynamically unstable. Due to the rapid bio-reduction, assembly and room temperature sintering, these least protected NPs led to formation of large anisotropic Au-NPs. The freshly developed anisotropic bigger size NPs suffered shrinking, with minimized surface energy, resulting in smooth angled large anisotropic particles. Similar results were reported recently in the synthesis of NPs using honey [3] and *Coleus amboinicus* lour [29]. The initial phase of bio-reduction, spherical small sized NPs were formed due to availability of sufficient biomolecules for protection. Therefore, TEM image showed that the nearly spherical shape NPs were abundant compared to the bigger size anisotropic NPs.

4. X-ray Diffraction Analysis

Crystalline structure and composition of NPs were confirmed by XRD analysis. Fig. 4(a) and (b) represented the characteristic diffraction peaks corresponding to (111), (200), (220), (311) plane of Au-NPs and Ag-NPs were located at 2θ position 38.21°, 44.33°, 64.75°, 77.66° and 38.16°, 44.39°, 64.60°, 77.50° respectively (JCPDS no. 04-0784, 04-0783). The ratio between (200) and (111) diffraction peak intensity calculated as 0.25 and 0.34 for Au-NPs and Ag-NPs, respectively indicating predominant orientation of (111) plane.

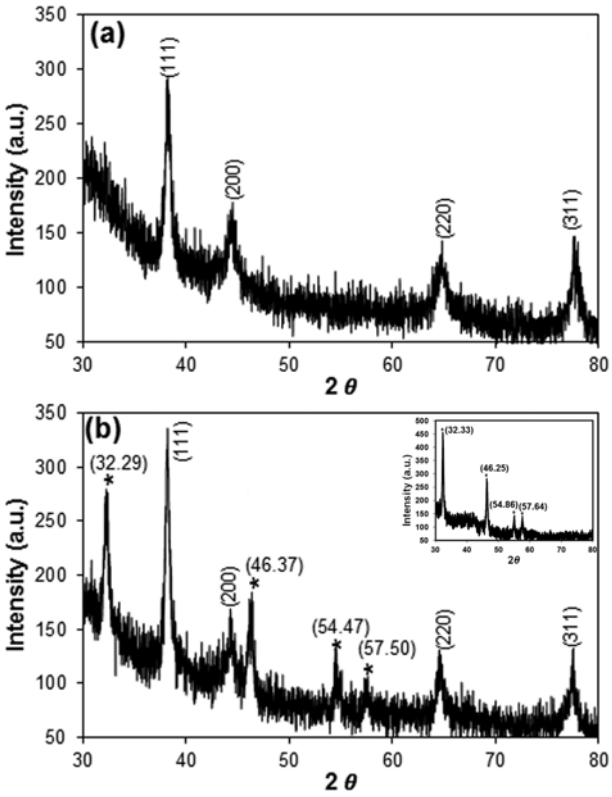

Fig. 4. XRD pattern of (a) Au-NPs (b) Ag-NPs (inset represents XRD pattern of *C. aurantifolia* peel extract).

The lattice constant 4.079 and 4.084 Å calculated from this data was confirmed the faced center cubic (fcc) structure of synthesized Au-NPs and Ag-NPs, respectively.

The significant broadening of the diffraction peaks, ascribed to the nano-metric size range of synthesized particles, while the strong and sharp nature of diffraction peaks indicated the high-quality crystallization of the synthesized NPs. No additional peaks were observed in the XRD pattern of Au-NPs revealed high purity. However, few additional unidentified sharp peaks (*) with high intensity were also accompanied with crystalline Ag-NPs at 32.29°, 46.37°, 54.47°, 57.50°. These sharp peaks were due to the crystallization of organic compounds of *C. aurantifolia* peel extract on the surface of the Ag-NPs or vice-versa, which revealed strong X-ray scattering centers in the crystalline phase. For further confirmation of crystallization of organic compounds on the surface of Ag-NPs or vice-versa, XRD analysis was carried out for peel extract of *C. aurantifolia*. In the inset of Fig. 4(b), the XRD spectrum of a film cast from peel extract represented strong sharp peaks with high intensity at 32.33°, 46.25°, 54.86° and 57.64° positions suggested the presence of a crystalline phase of some bio-organic compounds of peel extract [30]. Comparison of this spectrum with XRD spectrum of Ag-NPs indicated slight shift (<0.5°) in peak position with decrease in peak intensity, which was due to the bio-organic compounds of peel extract on the surface of the Ag-NPs or vice-versa. Similar result was also reported earlier for biosynthesis of Ag-NPs using different plant resources [7,30]. The average crystallite size calculated by Scherrer equation using the line width of the (111) diffraction peaks were

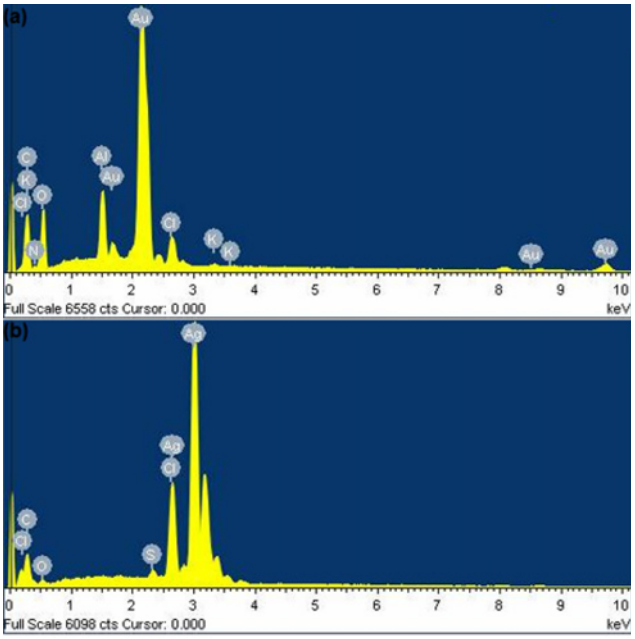

Fig. 5. EDX spectra of (a) Au-NPs (b) Ag-NPs.

obtained as 22 and 31 nm for Au-NPs and Ag-NPs, respectively, corroborate with the results of TEM analysis.

5. Energy Dispersive X-ray Spectroscopy Analysis

The appearance of intense absorption peaks approximately at 2.20 and 3 keV was due to the SPR of metallic Au and Ag nanocrystallites (Fig. 5(a), (b)). Few light signals of Au-NPs were also observed at around 1.7, 8.6 and 9.8 keV. Surface adsorption of organic moieties confirmed by the presence of oxygen and carbon signals. The appearance of Al signal observed due to the use of aluminum grid in analysis. X-ray emission from different minerals of *C. aurantifolia* peel extract reflected by the presence of N, K, Cl and S signals.

6. Fourier Transform Infrared Spectroscopic Analysis

To determine the functional groups present in *C. aurantifolia* peel extract and to predict their role in the biosynthesis of NPs, FTIR analysis was carried out. The *C. aurantifolia* peel extract spectra showed number of peaks, which was reflected a complex nature of the peel extract. The change in peak intensity and position in different regions of the spectrum of the *C. aurantifolia* peel extract to Au-NPs and Ag-NPs were shown in Fig. 6(a), (b), (c). The slight shift observed in the following peaks: 3,411 to 3,424 and 3,429 cm^{-1}, 2,920 to 2,922 and 2,921 cm^{-1}, 1,613 to 1,640 and 1,628 cm^{-1} and 1,028 to 1,027 and 1,023 cm^{-1}. The difference in magnitude of peaks intensity and position in both NPs was attributed to the difference in nature of the co-ordination with different metal surface.

The peak shift after bio-reduction in broad and intense absorption peak of *C. aurantifolia* peel extract at around 3,411 cm^{-1} indicated the involvement of O-H functional group of phenols and carboxylic acids for the synthesis of NPs. The peak shift in 2,920 cm^{-1} stretching vibration was attributed to the possible involvement of C-H stretching vibration of aliphatic acids in NPs synthesis. The peaks observed at 1,613 cm^{-1} and 1,444 cm^{-1} were due to asymmetric and symmetric stretching vibrations of C=O in carboxylic groups. The shift in 1,613 cm^{-1} peak and disappearance of 1,444

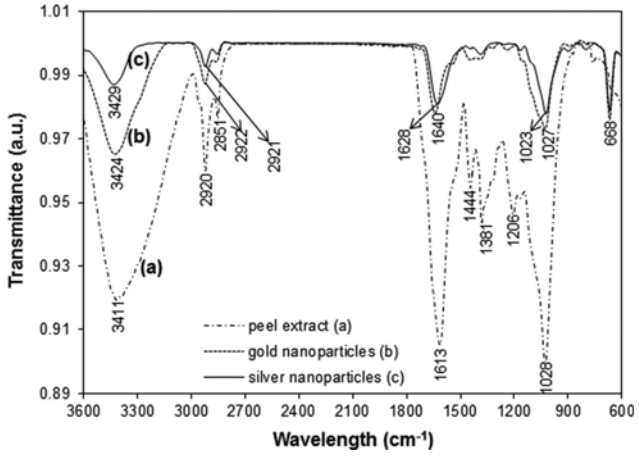

Fig. 6. FTIR spectra of (a) Au-NPs (b) Ag-NPs (c) *C. aurantifolia* peel extract before bio-reduction.

cm^{-1} peak indicated the involvement of C=O group in NPs synthesis. The stretching vibration present in *C. aurantifolia* peel extract at around 1,381 cm^{-1} and 1,206 cm^{-1} represented C=O stretching vibrations of carboxylic acid and C-OH vibrations of polyols. The disappearance of these two peaks in FTIR spectra of NPs indicated the involvement of carboxylic acid and polyols in NPs synthesis. The shift in stretching vibration present at 1,028 cm^{-1} suggested the involvement of C-OH group of carboxylic acids in NPs synthesis. After bio-reduction the peak intensity was reduced in FTIR spectra of both NPs. FTIR spectra indicated that the different functional groups (O-H, C-H, C=O and C-OH) were used for bio-reduction of the precursors along with shape evolution and stabilization of NPs. Citrus peels principally consist of citric acid, ascorbic acid along with different polyphenolic compounds (flavonoid and phenolic acid), with excellent reducing properties [31,32]. These components mainly contain carboxyl and hydroxyl groups. FTIR spectra implied that these bio-organic compounds were the probable bio-reducing and capping agents for NPs, causing steric hindrance and electrostatic repulsion to stabilized NPs against the van der Waals forces of attraction. Synthesized NPs possessed negative surface

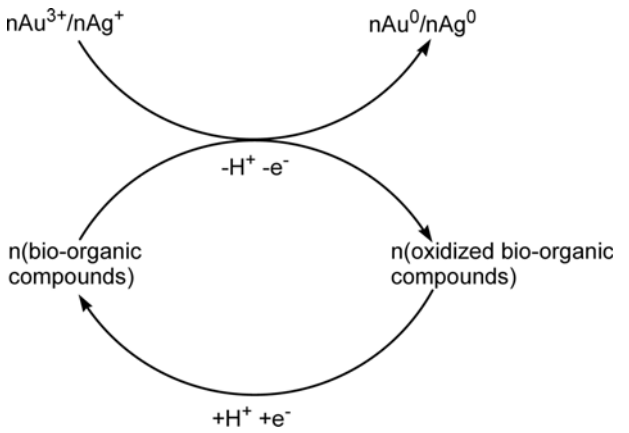

Scheme 1. Possible mechanism involved in the bio-reduction of Au^{3+} and Ag^{+} metal ion using mixture of bio-organic compounds of *C. aurantifolia* peel extract.

Table 1. Bio-organic compounds and their oxidized products

S. no.	Bio-organic compounds	Structure of bio-organic compounds	Structure of oxidized products	Reference
1	Citric acid	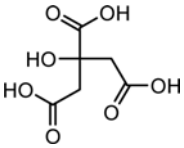	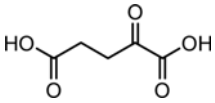	[34]
2	Ascorbic acid	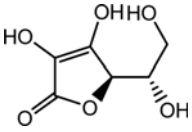	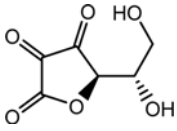	[35]
3	Gallic acid	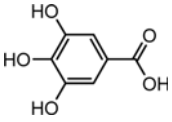	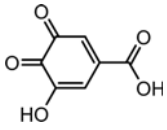	[36]
4	Protocatechuic acid	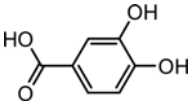	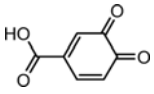	[36]
5	Catechin	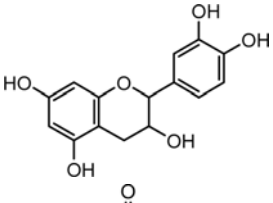	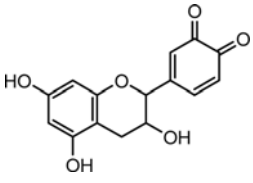	[36]
6	Ellagic acid	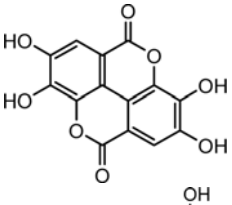	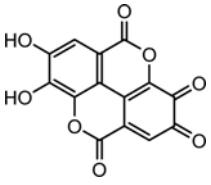	[37]
7	Quercetin	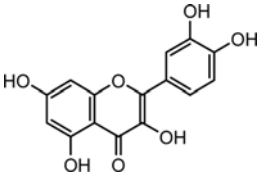	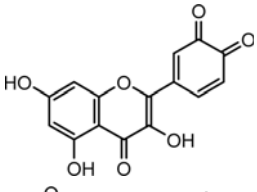	[37]
8	Caffeic acid	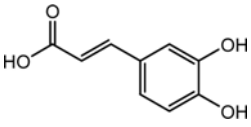	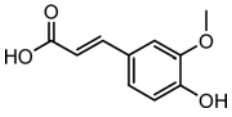	[38]

charge due to the adsorbed bio-organic compounds. The observed negative ζ potential of NPs also suggested capping of NPs by bio-organic compounds.

Citrus peel represented a complex storehouse of many antioxidant bio-organic compounds like citric acid, ascorbic acid and polyphenolic compounds [31,32]. The -OH and C=O groups of these bio-organic compounds showed strong ability to bind metal ions [33]. The antioxidant potential of these compounds was due to their ability to donate electron/hydrogen atom. This reactive hydrogen is responsible for bio-reduction of metal ions to zero valent form and number of bio-organic compounds acts synergistically in bio-reduction reaction and produces corresponding oxidized [34-38] compounds. After considering all the facts, the plausible general mechanism of bio-reduction reaction (redox reaction) with mixture of bio-organic compounds, was illustrated in Scheme 1. The structure of different bio-organic compounds and their oxidized products obtained during bio-reduction reaction are shown in Table 1.

7. Catalytic Hydrogenation of 4-NA using Au-NPs and Ag-NPs

The NPs with (111) facets with sharp edges and corners were catalytically more active [39]. In the present study, the XRD pattern showed predominant orientation of (111) plane in both synthesized NPs. The as-prepared Au-NPs and Ag-NPs were expected to show good catalytic activity. Kong et al. [40] proposed that the hydrogenation of 4-NA to 4-PDA by $NaBH_4$ was quite slow in the absence of catalyst. To verify the catalytic activity of the as-synthesized Au-NPs and Ag-NPs, a similar reaction was chosen as a model reaction. It was observed that the absorption spectrum of a mixture of 4-NA with $NaBH_4$ showed a band at 380 nm correspond-

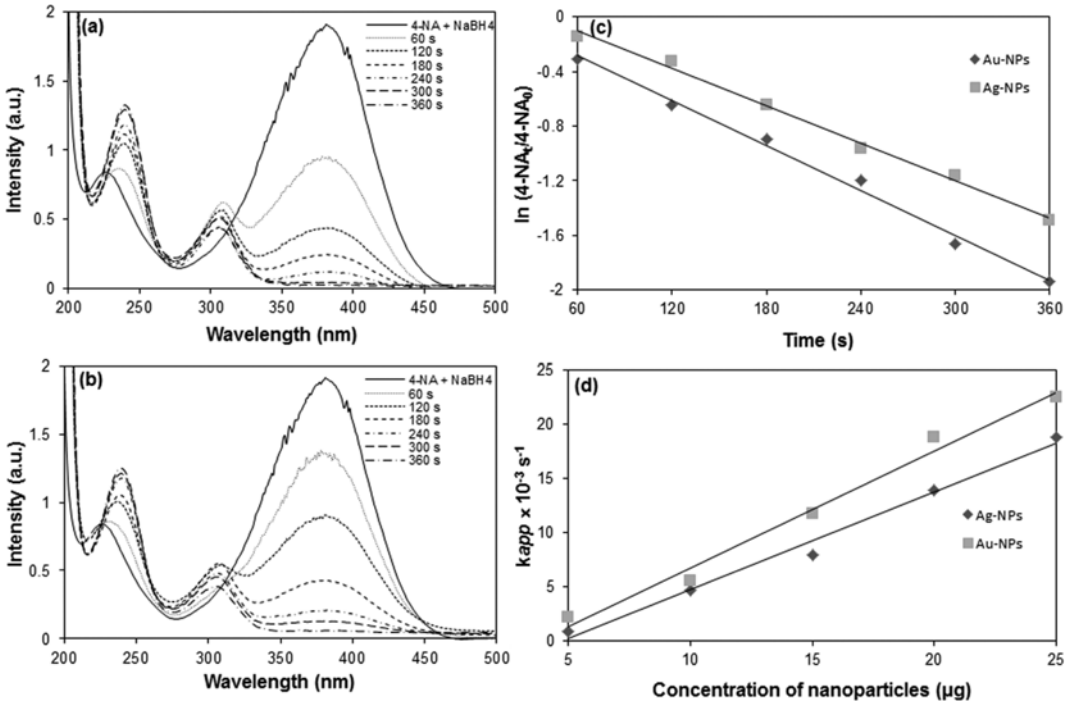

Fig. 7. Time-dependent absorption spectra for the catalytic hydrogenation of 4-NA by $NaBH_4$ in the presence of (a) Au-NPs (b) Ag-NPs (c) plot of ln(4-NA_t/4-NA_0) vs. reaction time (d) plot of the rate of hydrogenation of 4-NA vs. concentration of NPs.

ing to intermolecular charge transfer of 4-NA as in Fig. 7(a), (b). At the same time, two new peaks gradually developed at 240 and 310 nm, corresponding to the formation of 4-PDA in the solution after the addition of Au-NPs and Ag-NPs. Meantime, it was accompanied with flattening of the characteristic band at 380 nm, indicating the completion of the 4-NA hydrogenation reaction.

In this hydrogenation process, the concentration of $NaBH_4$ in the reaction mixture exceeded the concentration of 4-NA, and the logarithm of the absorbance of 4-NA at 380 nm ln(4-NA_t/4-NA_0) linearly decreased with reaction time. The apparent rate constant (k_{app}, min^{-1}) of the catalytic hydrogenation was calculated from a linear regression of the slope of ln(4-NA_t/4-NA_0) versus time (Fig. 7(c)). The plot obtained was a straight line, indicating that the hydrogenation reaction followed pseudo-first-order-kinetics. The pseudo-first-order rate constant, k_{app} was calculated to be 5.5×10^{-3} and 4.6×10^{-3} s^{-1} for the Au-NPs and Ag-NPs, respectively.

The effect on the concentration of NPs on the 4-NA hydrogenation rate was determined by varying the amounts of NPs (5 µg-25 µg), while keeping the other parameters constant. Fig. 7(d) shows a linear increase in hydrogenation rate, with an increase in both NPs concentration. This was due to the accessibility of more surface area, which ultimately increased the interaction sites of NPs, and finally hydrogenation rate of 4-NA conversion increased. This observation was justified by the fact that NPs facilitated catalytic activity through the surface reaction phenomenon [41]. The concentration of NPs used in the present system for 4-NA hydrogenation was much less than the earlier reported polymer supported chemically synthesized NPs. However, this result revealed that the hydrogenation reaction rate was comparable to earlier reports [42, 43]. Therefore, these results elucidated biologically synthesized NPs as an economical and biocompatible catalyst for 4-NA hydrogenation.

CONCLUSION

Au-NPs and Ag-NPs were synthesized biometrically using agro-industrial waste *C. aurantifolia* peel extract at room temperature. Biosynthesis of NPs started within 2 min of incubation time. Citric acid, ascorbic acid along with polyphenolic components of peel extract act synergistically for the bio-reduction of precursor salts. Both NPs are found efficient catalysts for the hydrogenation of anthropogenic pollutants 4-NA. These findings suggest biosynthesized NPs as cost effective and eco-friendly alternative for environmental bioremediation.

ACKNOWLEDGEMENTS

The authors are grateful to the Sophisticated Analytical Instrument Facility (SAIF), IIT Bombay for providing the research facilities for characterizations of samples.

REFERENCES

1. J. Y. Song and B. S. Kim, *Korean J. Chem. Eng.*, **25**, 808 (2008).
2. M. Ghaffari-Moghaddam, R. Hadi-Dabanlou, M. Khajeh, M. Rakhshanipour and K. Shameli, *Korean J. Chem. Eng.*, **31**, 548 (2014).
3. D. Philip, *Spectrochim. Acta A*, **73**, 650 (2009).
4. V. Amendola, O. M. Bakr and F. Stellacci, *Plasmonics*, **5**, 85 (2010).
5. X. Du, J. He, J. Zhu, L. Sun and S. An, *Appl. Surf. Sci.*, **258**, 2717 (2012).

6. R. L. Oliveira, P. K. Kiyohara and L. M. Rossi, *Green Chem.*, **12**, 144 (2010).
7. M. Vanaja and G. Annadurai, *Appl. Nanosci.*, **3**, 217 (2013).
8. K. Velayutham, A. A. Rahuman, G. Rajakumar, S. M. Roopan, G. Elango, C. Kamaraj, S. Marimuthu, T. Santhoshkumar, M. Iyappan and C. Siva, *Asian Pac. J. Trop. Med.*, **6**, 95 (2013).
9. C. Jayaseelan, R. Ramkumar, A. A. Rahuman and P. Perumal, *Ind. Crops Prod.*, **45**, 423 (2013).
10. R. K. Das, N. Gogoi and U. Bora, *Bioprocess Biosyst. Eng.*, **34**, 615 (2011).
11. A. I. Lukman, B. Gong, C. E. Marjo, U. Roessner and A. T. Harris, *J. Colloid Interface Sci.*, **353**, 433 (2011).
12. P. Dauthal and M. Mukhopadhyay, *Ind. Eng. Chem. Res.*, **51**, 13014 (2012).
13. N. Yang and W. H. Li, *Ind. Crops Prod.*, **48**, 81 (2013).
14. S. Kaviya, J. Santhanalakshmi, B. Viswanathan, J. Muthumary and K. Srinivasan, *Spectrochim. Acta A*, **79**, 594 (2011).
15. M. V. Sujitha and S. Kannan, *Spectrochim. Acta A*, **102**, 15 (2013).
16. R. G. Haverkamp and A. T. Marshall, *J. Nanopart. Res.*, **11**, 1453 (2009).
17. V. V. Makarov, S. S. Makarova, A. J. Love, O. V. Sinitsyna, A. O. Dudnik, I. V. Yaminsky, M. E. Taliansky and N. O. Kalinina, *Langmuir*, **30**, 5982 (2014).
18. S. Yallappa, J. Manjanna, M. A. Sindhe, N. D. Satyanarayan, S. N. Pramod and K. Nagaraja, *Spectrochim. Acta A*, **110**, 108 (2013).
19. E. C. Njagi, H. Huang, L. Stafford, H. Genuino, H. M. Galindo, J. B. Collins, G. E. Hoag and S. L. Suib, *Langmuir*, **27**, 264 (2011).
20. V. Reddy, R. S. Torati, S. Oh and C. Kim, *Ind. Eng. Chem. Res.*, **52**, 556 (2013).
21. A. Gangula, R. Podila, M. Ramakrishna, L. Karanam, C. Janardhana and A. M. Rao, *Langmuir*, **27**, 15268 (2011).
22. X. Bai, Y. Gao, H. G. Liu and L. Zheng, *J. Phys. Chem. C*, **113**, 17730 (2009).
23. W. Liu, X. Yang and L. Xie, *J. Colloid Interface Sci.*, **313**, 494 (2007).
24. S. E. Lyubimov, A. A. Vasilév, A. A. Korlyukov, M. M. Ilyin, S. A. Pisarev, V. V. Matveev, A. E. Chalykh, S. G. Zlotin and V. A. Davankov, *React. Funct. Polym.*, **69**, 755 (2009).
25. N. S. Lawrence, E. L. Beckett, J. Davis and R. G. Compton, *Analyst*, **126**, 1897 (2001).
26. P. B. Sulekha, R. Joseph and S. Prathapan, *J. Appl. Polym. Sci.*, **81**, 2183 (2001).
27. M. Umadevi, M. R. Bindhu and V. J. Sathe, *Mater. Sci. Technol.*, **29**, 317 (2013).
28. I. O. Sosa, C. Noguez and R. G. Barrera, *J. Phys. Chem. B*, **107**, 6269 (2003).
29. K. B. Narayanan and N. Sakthivel, *Mater. Charact.*, **61**, 1232 (2010).
30. S. S. Shankar, A. Ahmad and M. Sastry, *Biotechnol. Prog.*, **19**, 1627 (2003).
31. M. R. Loizzo, R. Tundis, M. Bonesi, F. Menichini, D. D. Luca, C. Colica and F. Menichini, *J. Sci. Food Agric.*, **92**, 2960 (2012).
32. J. A. Vinson, X. Su, L. Zubik and P. Bose, *J. Agric. Food Chem.*, **49**, 5315 (2001).
33. J. F. Moran, R. V. Klucas, R. J. Grayer, J. Abian and M. Becana, *Free Radic. Biol. Med.*, **22,** 861 (1997).
34. R. Konwarh, B. Gogoi, R. Philip, M. A. Laskar and N. Karak, *Colloids Surf., B*, **84**, 338 (2011).
35. A. K. Jha, K. Prasad, K. Prasad and A. R. Kulkarni, *Colloids Surf., B*, **73**, 219 (2009).
36. P. Dauthal and M. Mukhopadhyay, *Ind. Eng. Chem. Res.*, **52**, 18131 (2013).
37. P. Dauthal and M. Mukhopadhyay, *J. Ind. Eng. Chem.*, DOI:10.1016/j.jiec.2014.07.009.
38. S. A. Aromal, V. K. Vidhu and D. Philip, *Spectrochim. Acta A*, **85**, 99 (2012).
39. R. Narayanan and M. A. El-Sayed, *J. Phys. Chem. B*, **109**, 12663 (2005).
40. L. Kong, X. Lu, E. Jin, S. Jiang, X. Bian, W. Zhang and C. Wang, *J. Solid State Chem.*, **182**, 2081 (2009).
41. A. Murugadoss and A. Chattopadhyay, *J. Phys. Chem. C*, **112**, 11265 (2008).
42. H. Jia, X. Gao, Z. Chen, G. Liu, X. Zhang, H. Yan, H. Zhou and L. Zheng, *CrystEngComm*, **14**, 7600 (2012).
43. Q. Zhou, G. Qian, Y. Li, G. Zhao, Y. Chao and J. Zheng, *Thin Solid Films,* **516**, 953 (2008).